Electronic Supplementary Information (ESI)

Foaming Photothermal Inks for Direct-Ink Writing: Hierarchical Design and Enhanced Solar-Powered Interfacial Evaporation

Jie Gao,[a] Ke Shao,[a] Jingjing Li,[a] Na Li,[a] Shuxue Wang,[a] Xiaochun Wu,[a] Petri Murto,[b] Zhihang Wang,*[c] Yingtang Zhou,*[d] & Xiaofeng Xu*[a]

[a] College of Materials Science and Engineering, Ocean University of China, Qingdao 266100, China.

[b] Yusuf Hamied Department of Chemistry, University of Cambridge, Cambridge, CB2 1EW, United Kingdom.

[c] Department of Materials Science and Metallurgy, University of Cambridge, Cambridge, CB3 0FS, United Kingdom

[d] National Engineering Research Center for Marine Aquaculture, Marine Science and Technology College, Zhejiang Ocean University, Zhoushan 316004, China

* Corresponding authors: X. Xu, email: xuxiaofeng@ouc.edu.cn

Y. Zhou, email: zhouyingtang@zjou.edu.cn

Z. Wang, email: zw428@cam.ac.uk

Table of Contents

1. Materials

Bacterial cellulose nanofibers (CNFs) were purchased from Guilin Qihong Tech. Co., Ltd. Sodium alginate (SA) and carbon particles (CB) were purchased from Shanghai Macklin Biochemical Co., Ltd, China. Polyvinyl alcohol (PVA), glutaraldehyde (GA, crosslinker, 50 wt% in H_2O), calcium chloride ($CaCl_2$, 99%) and hydrochloric acid (HCl, 35 wt%) were purchased from Sinopharm Chemical Reagent Co., Ltd, China.

2. Materials characterization

Apparent viscosities of precursor gels were measured via a high-sensitivity rotational viscometer (NDJ-79A, Shanghai Changji). The fourier-transform infrared (FTIR) spectra were measured via a FTIR Spectrometer (iS50 FT-IR, Thermo Fisher Scientific). Contact angles were measured via a contact angle goniometer (JC2000DM, Powereach) by using 4 μL of water droplet as an indicator. The absorption spectra were obtained from a UV−Vis−NIR spectrometer (LAMBDA 1050+, PerkinElmer) with an integrating sphere. The absorptance at each wavelength is defined by $1 - T - R$, where T and R are the corresponding transmittance and reflectance, respectively. The densities, porosity and saturated water contents were measured by using a high-precision density meter (AU-120PF, Quarrz). The morphologies and elemental mapping were characterized by a scanning electron microscope (VEGA3, TESCAN) in combination with energy dispersive X-ray spectrometry. 3D optical microscope images of aerogels were characterized via a 3D laser scanning confocal microscope (VK-X260K, Keyence). TDS and salinity were examined by using a high-precision salinometer (Cond 7110, WTW). Polarized optical microscopy (POM) was conducted on a Leica DM2500P equipped with a CCD camera and cross-polarizers. The Micro-CT images of internal structure characterization were shot and reconstructed through a microcomputed tomography (Micro-CT) equipment (Skyscan 1272, Bruker, Germany). Compressive stress−strain curves of aerogels were measured using a mechanical testing system equipped

with a digital force gauge (M5-100, MARK-10) and a force test stand (ESM303, MARK-10).
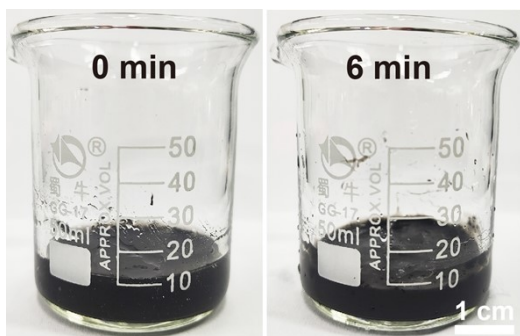
3. Foaming characterization

Figure S1. Digital photographs of the CNF-SA gel before and after the foaming procedure.
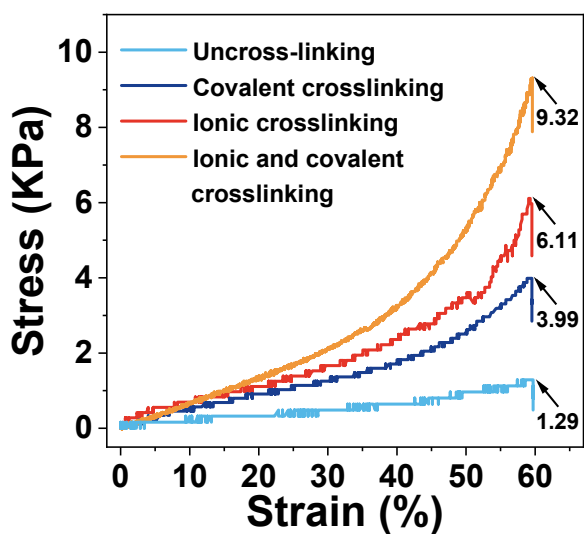
4. Compression testing

Figure S2. Effect of cross-linking state on compression properties.

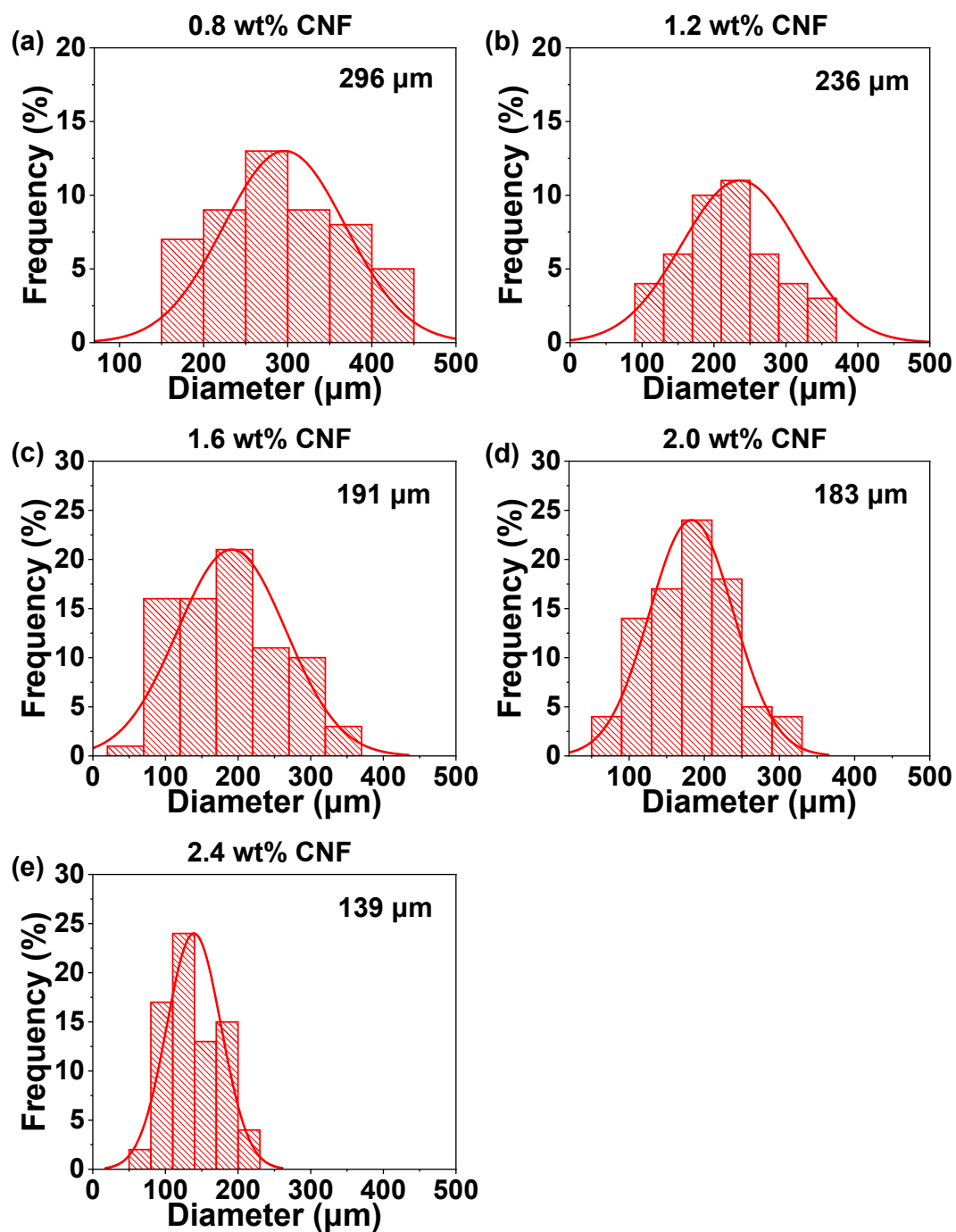## 5. Pore size distribution of hydrogel foams

Figure S3. Pore size distribution of hydrogel foams fabricated at different CNF concentrations.
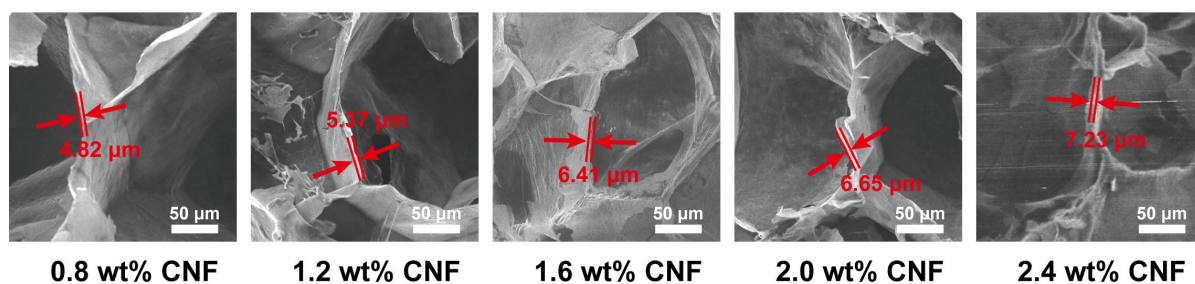
6. SEM images of aerogel foams

| 0.8 wt% CNF | 1.2 wt% CNF | 1.6 wt% CNF | 2.0 wt% CNF | 2.4 wt% CNF |

Figure S4. SEM images of aerogel foams fabricated at different CNF concentrations.

7. Foaming volume decay of foaming gels

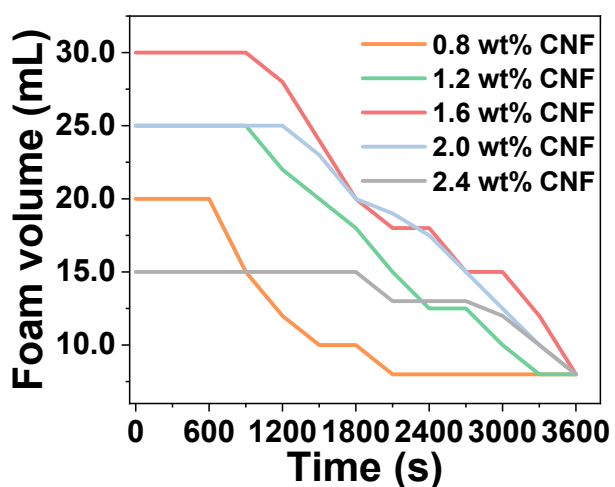**Figure S5**. Foam volume decay at different CNF concentrations.

8. Digital photographs of foaming gels

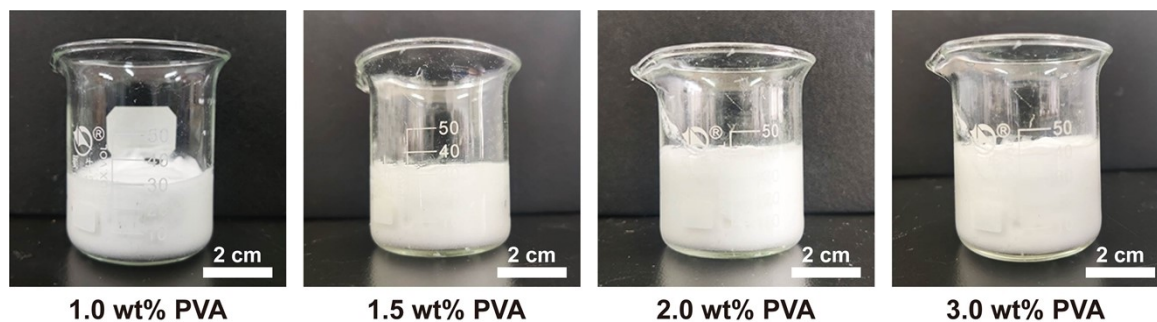| 1.0 wt% PVA | 1.5 wt% PVA | 2.0 wt% PVA | 3.0 wt% PVA |

Figure S6. Digital photographs of foaming gels fabricated at different PVA concentrations.

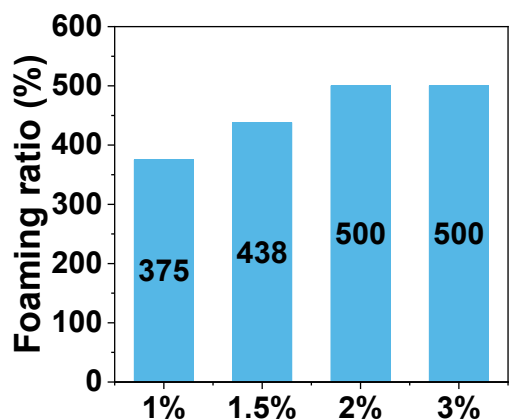## 9. Characterization of foaming volumes

Figure S7. Foaming ratios of the gels fabricated at different PVA concentrations.

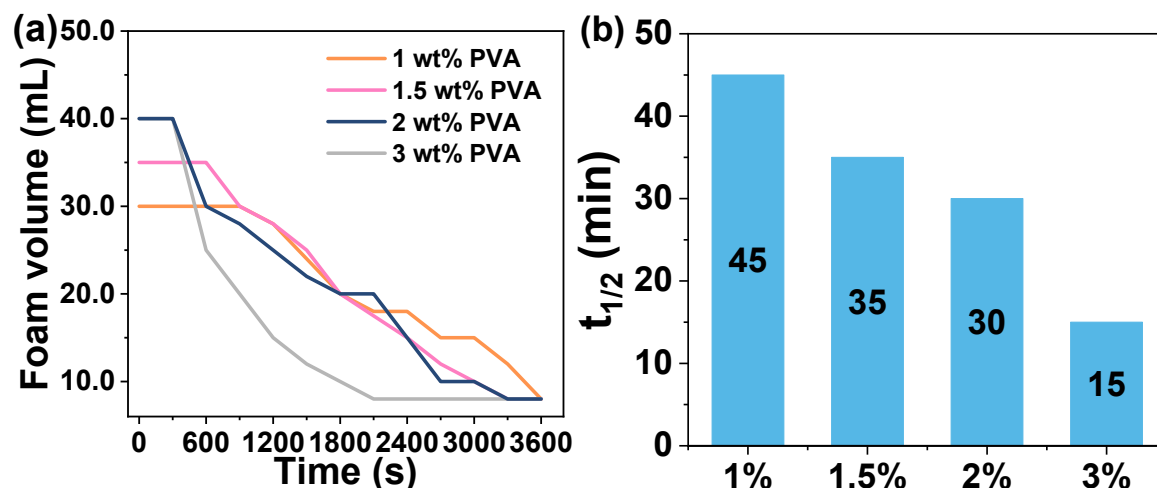## 10. Characterization of foaming stability

Figure S8. (a) Foaming volume decay and (b) $t_{1/2}$ of foaming gels fabricated at different PVA concentrations.
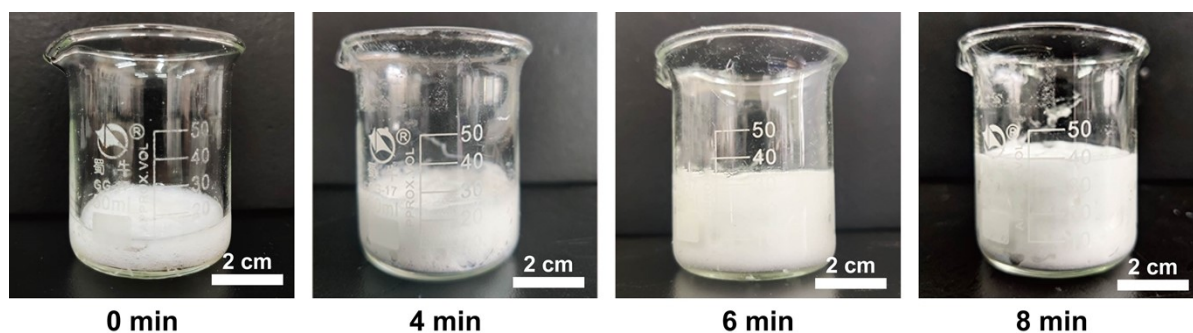
11. Digital photographs of foaming gels

Figure S9. Digital photographs of foaming gels fabricated at different foaming time.
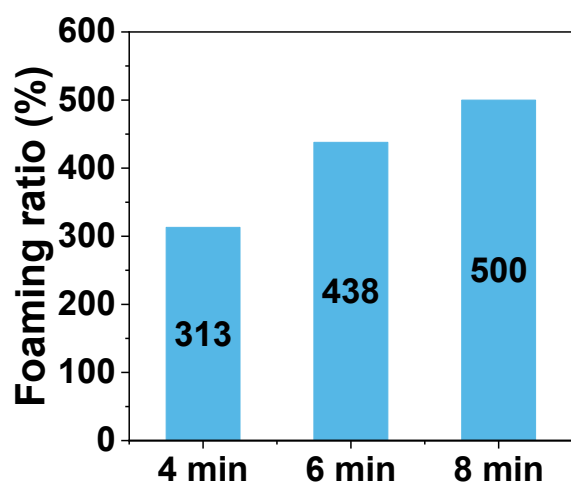
12. Characterization of foaming volumes

Figure S10. Foaming ratios of the gels fabricated at different foaming time.
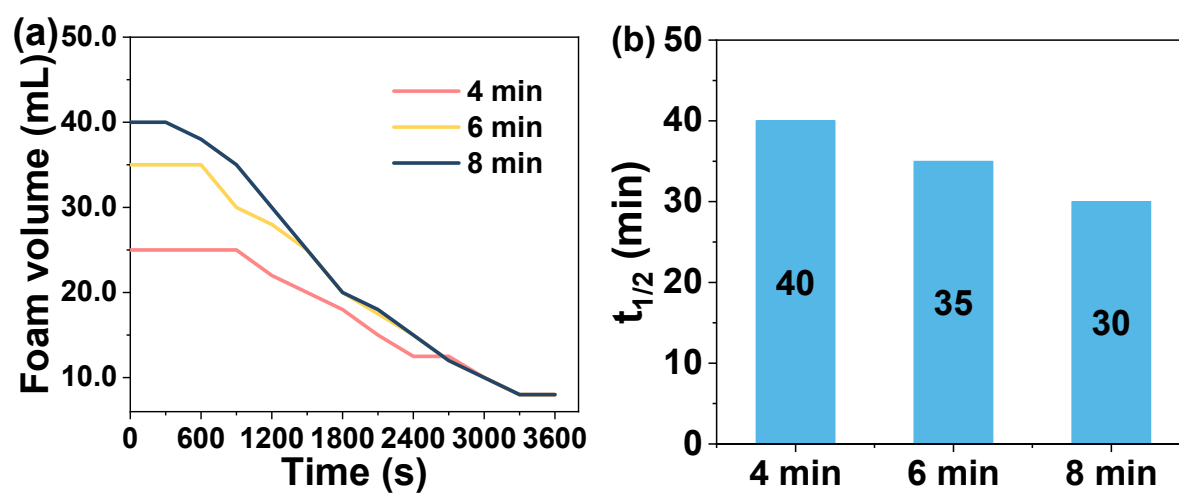
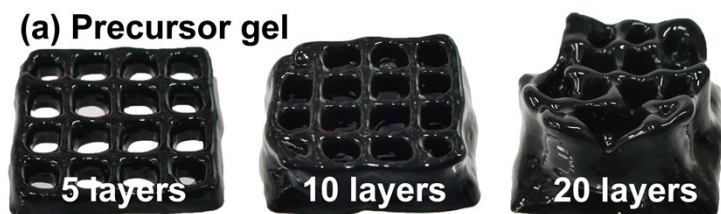## 13. Characterization of foaming stability

Figure S11. (a) Foaming volume decay and (b) $t_{1/2}$ of foaming gels fabricated at different foaming time.
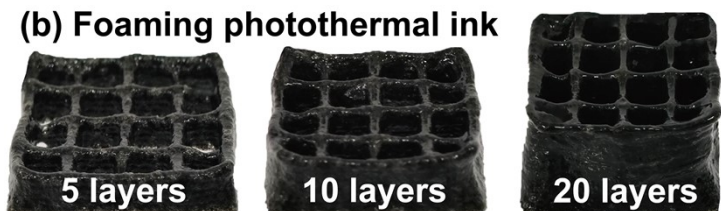
14. Digital photographs

Figure S12. Digital photographs of 3D structures printed based on the (a) precursor gel and (b) foaming photothermal ink.
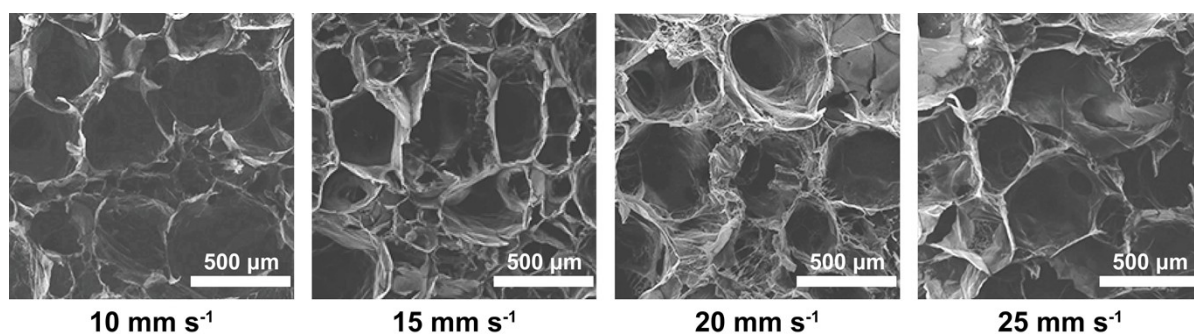

15. SEM images of 3D-printed filaments

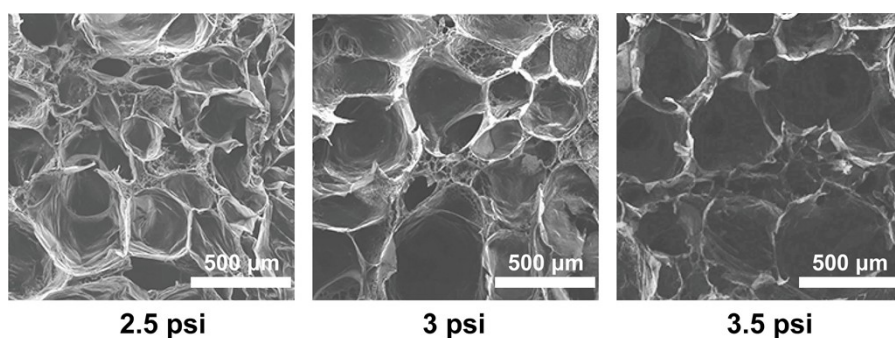**Figure S13**. SEM images of 3D-printed filaments fabricated at different needle movement speeds.

Figure S14. SEM images of 3D-printed filaments fabricated at different extrusion pressures.
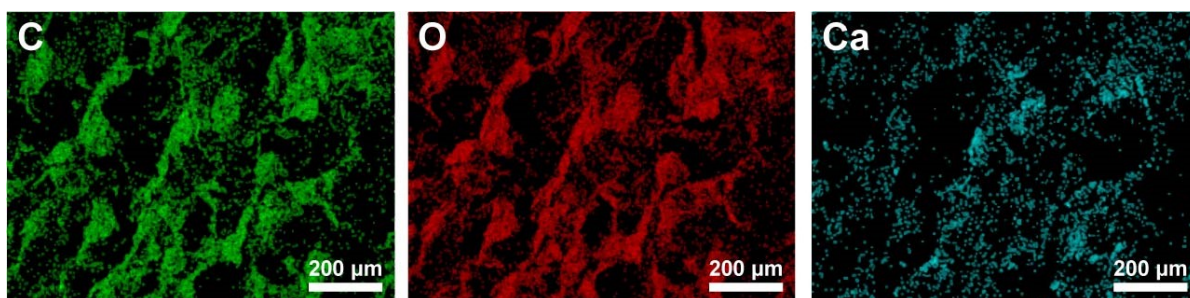
16. EDS characterization

Figure S15. EDS images of characteristic elements in 3D-printed filaments.
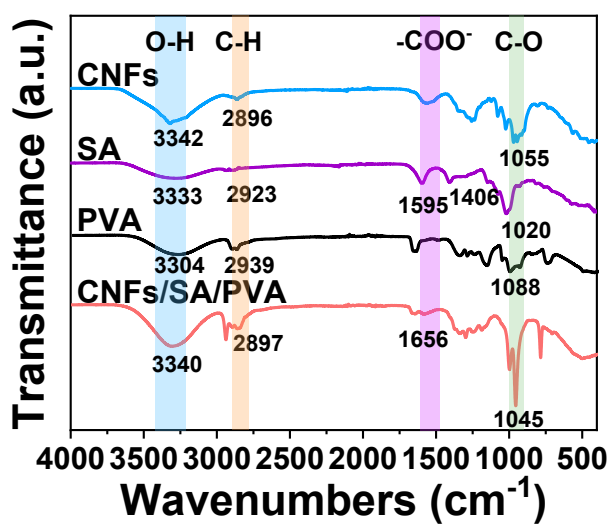
17. FTIR characterization

Figure S16. FTIR spectra of CNFs, SA, PVA and CNFs/SA/PVA composite.

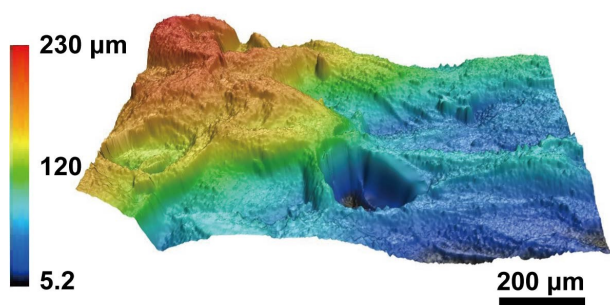## 18. 3D laser scanning confocal microscopy

Figure S17. 3D laser scanning confocal microscope images.
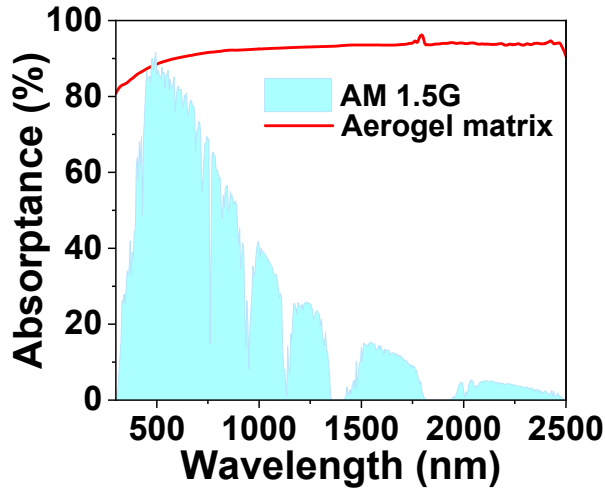
19. Absorptance characterization

Figure S18. Absorption spectrum of a 3D-printed aerogel matrix.

The transmission and reflection spectra of the aerogel matrix over the whole solar spectrum (250 − 2500 nm) were measured using an UV−Vis−NIR spectrophotometer equipped with an integrating sphere. According to Kirchhoff's law, the absorption spectrum can be obtained through the formula: A = 1 − R − T. Therefore, the absorptance (A_t) of the aerogel matrix across the full solar spectrum can be calculated using equation S1,

$$A_t = \frac{\int A \cdot S \cdot d\lambda}{\int S \cdot d\lambda} \times 100\% \tag{S1}$$

where S is solar spectral irradiance (W m^{-2} nm^{-1}) and λ is wavelength (nm).

20. IR images

(a) Bulk water

Initial	10 min	1 h
25.8 °C	26.7 °C	28.5 °C
25.8 °C	26.4 °C	28.1 °C

32 °C – 25 °C

(d) SG3

Initial	10 min	1 h
25.7 °C	30.5 °C	31.5 °C
24.9 °C	25.0 °C	25.1 °C

35 °C – 22 °C

(b) SG1

Initial	10 min	1 h
26.5 °C	37.9 °C	41 °C
25.7 °C	25.9 °C	26.3 °C

45 °C – 25 °C

(e) SG4

Initial	10 min	1 h
27.2 °C	31.7 °C	32.1 °C
24.8 °C	24.9 °C	25.1 °C

35 °C – 22 °C

(c) SG2

Initial	10 min	1 h
25.8 °C	29.9 °C	31.3 °C
23.6 °C	23.7 °C	24.0 °C

35 °C – 22 °C

(f) SG5

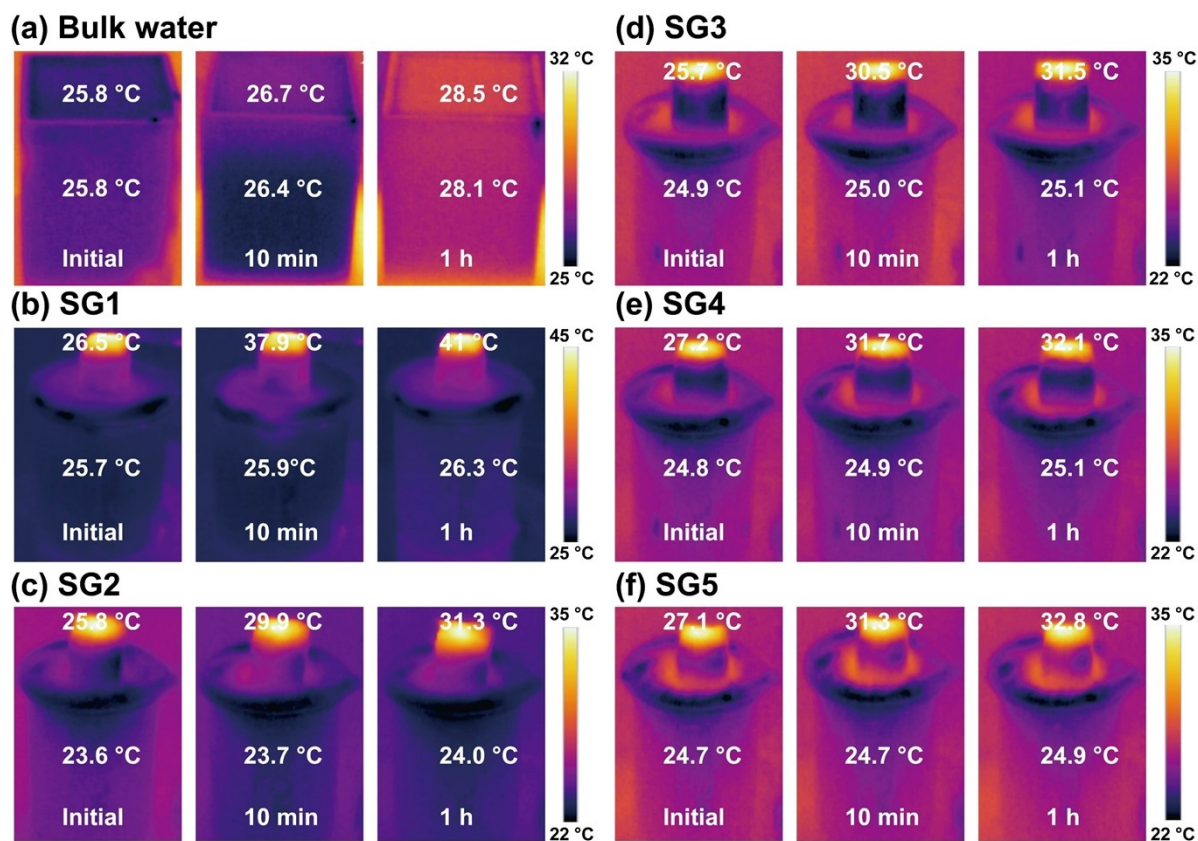| Initial	10 min	1 h
27.1 °C	31.3 °C	32.8 °C
24.7 °C	24.7 °C	24.9 °C

35 °C – 22 °C

Figure S19. IR images of bulk water and interfacial steam generators under one sun.

21. Water evaporation measurements

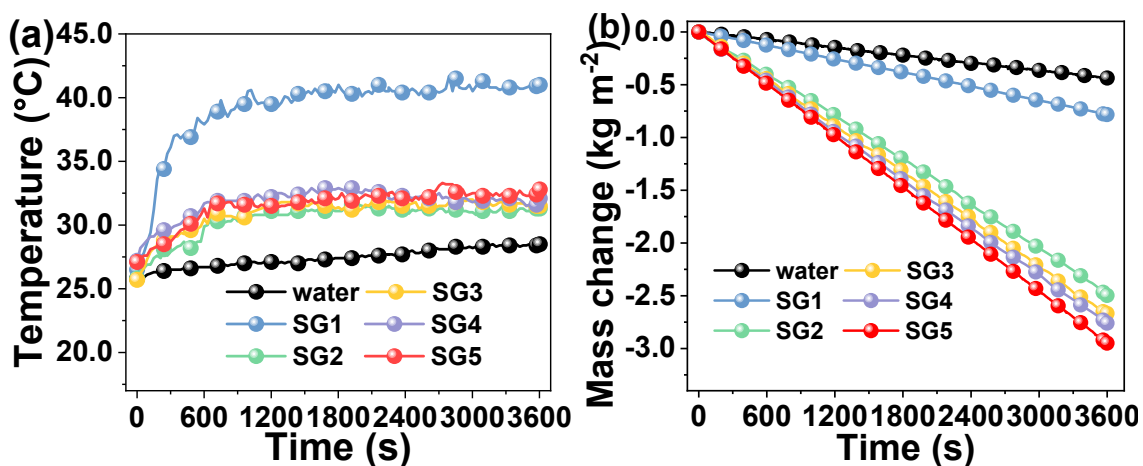**Figure S20**. (a) Average surface temperature and (b) mass changes of water over 1 h under 1 sun.

22. Summary of 3D-printed interfacial SGs

Table S1. Material components and performance of interfacial SGs in recent reports.

Ref.	Symbol	Materials	Evaporation rate (kg m^{-2} h^{-1})
1		Acrylonitrile-styrene-acrylate	1.71
2		Self-made UV curable resin Carbon nanotubes (CNTs)	2.63
3		Silica Resorcinol−formaldehyde Polyimide	1.57
4		PDA(GF/C)/PVA/PVP	1.60
5		UV-curable acrylic ester resin Carbon nanofibers	1.64
6		MG@Silica	2.40
7		Polyimide/MXene	2.17
8		Acrylic resin Amino epoxy resin Ultrafine graphene powder	2.67
9		Cellulose Carbon black (CB)	3.01
10		Cellulose/alginate/carbon black	1.33
11		Pyrrole/PLA	1.73
12		K-carrageenan (CG) Poly (diallyldimethylammoniumchloride) (PDADMAC) Carbon nanotubes (CNTs)	2.30
13		CNF/ Carbon black (CB)	0.97
14		CNF Carbon nanotubes (CNTs)	1.43
15		SCG/ Polypyrrole (PPy)/ Polylactic acid (PLA)	1.54
16		Invicta DL380 resin Activated carbon (AC) powder	1.91
17		Methacrylated TA/FeCl$_3$	1.96

18	⊖	Photoinitiator (PI) Hydroxyethyl cellulose (HEC) Poly(styrene-acrylic) (P(St-AA) Polypyrrole (PPy)	2.00
19	�	Flower-like Co_3O_4 Sodium alginate	2.028
20	▯	Ni-cellulose nanofiber (Ni-CNF) Graphene oxide (rGO)	2.08
21	◀	Polyvinyl alcohol (PVA) Carbon nanofibers (CNFs)	2.53
22	■	Al2O3 particles/Epoxy resin	2.60
23	▼	Electrospun polyacrylonitrile (PAN) Carbon nanotubes (CNTs)	2.62
24	▭	Carboxymethyl Cellulose Sodium (CMC-Na) Carbon nanotubes (CNTs) RSN-700 photosensitive resin	2.775
25	⬡	Poly (ethylene glycol) diacrylate (PEGDA) Carbon black (CB) Sodium alginate (SA) Sodium lignosulfonate (SL)	2.78
26	■	N-isopropylacrylamide Acrylamide monomer Sodium acrylate absorbent	3.14
27	●	PVA-PEG-CS/GO	3.50
28	◇	Bacterial cellulose (BC) Sodium alginate (SA) Carbon nanopowder (CB)	3.74
29	▷	Polylactic acid (PLA)	4.02
30	⬣	Phenol-formaldehyde resin (PF) grains	4.84

23. Summary of cost-effective interfacial SGs

Table S2. Cost-effectiveness of interfacial SGs in previous reports.

Ref.	Symbol	Structural components	Estimated cost of each component ($ m^{-2})	Total costs ($ m^{-2})	Evaporation rates (kg m^{-2} h^{-1})	Cost-effectiveness (g h^{-1} $^{-1}$)
31		1) Polypyrrole 2) Sodium alginate	741.4 2.86	744.2	1.447	1.9
32		1) Reduced graphene oxide 2) Silver nanowires 3) Sodium alginate 4) PU sponge	8.195 681.42 0.197 3.00	692.8	2.02	2.9
33		1) Waste newspaper 2) Chemical regents 3) PDDA-PFO/SiO2 coating	0.0871 193.0003 27.1361	220.22	1.691	7.7
34		1) Polyvinyl alcohol 2) Ti$_2$O$_3$	11.60 281.61	293.2	3.6	12.3
35		1) Sodium alginate 2) MoS$_2$ 3) Melamine foam	0.94 81.25 3	85.19	1.81	21.2
36		1) Polyvinyl alcohol 2) Pyrrole 3) Ammonium persulfate	15.43 52.73 30.65	98.83	3.2	32.4
37		1) PVDF 2) WS$_2$	4.0 23.82	27.82	1.3	46.7
38		1) MXene/CIS	23	23	1.434	62.4
39		1) Polypyrene 2) Air-laid paper	10 10	20	1.35	67.5
40		1) Chitosan 2) Gelatin 3) Melanin-coated titania	0.43 0.17 10.72	11.32	1.3	114.8
41		1) Coal pitch 2) Formic acid (88%) 3) Hydrogen peroxide (30%) 4) Acetate fibers	0.0247 5.207 0.288 9.49	15.01	2.6	173.0
42		1) Polyvinyl alcohol 2) Konjac glucomannan 3) MOF derived absorber	7.71 0.08 7.15	14.9	3.2	215.0
43		1) PVA-203 2) Pyrrole 3) NPG seed	6.2 1.23 0.52	7.95	2.42	302.7
44		1) Tannic acid 2) PVP(K85) 3) Fe$_2$(SO$_4$)$_3$ 4) Tris	0.28 5.91 0.006 1.03	8.4	2.8	332.0

		5) HCl	0.018			
		6) PU sponge	1.18			
45		1) Pulp-natural rubber	4.78	4.78	1.62	338.9
46		1) Reduced graphene oxide 2) Rice-straw-derived cellulose 3) Sodium alginate	5.44 0.125 0.109	6.27	2.25	358.9
47		1) Potato starch 2) Squid ink powder	4.05 0.24	4.29	2.07	482.5
48		1) PVA/NCQD@Fe$_3$O$_4$	5.23	5.23	2.6	497.0
49		1) BCBF	3.6	3.6	2.8	778.0
50		1) Plant fibers 2) Chitosan 3) Baboo carbon black	0.1433 1.592 0.0192	1.75	1.38	788.6
51		1) Ceramic fiber 2) Carbon black 3) Activated carbon 4) PTFE 5) Deionized water	0.50 0.12 0.18 0.58 0.0004	1.38	1.7	1231.9
52		1) Sodium alginate (SA) 2) Polyvinyl alcohol (PVA) 3) CaCO$_3$ 4) Glutaraldehyde (GA) 5) Carbon particles (CB) 6)2-Hydroxypropyltrimethyl ammonium chloride chitosan (HACC)	0.35 0.25 0.0012 0.0023 0.11 0.064	0.78	2.1	2692.0
This work			SG1 0.392 3.469 0.001 0.222 0.063 9.408 0.182	13.555	0.78	57.5
		1) Sodium alginate (SA) 2) Polyvinyl alcohol (PVA) 3) HCl 4) Glutaraldehyde (GA) 5) Carbon particles (CB) 6) Bacterial cellulose nanofibers (CNF)	SG2 1.611 0.001 0.103 0.029 4.368 0.044 0.389	6.294	2.47	392.4
			SG3 0.0001 0.025 0.007 1.056	1.521	2.67	1755.4

		0.06			
		0.531			
⭐	SG4	0.0002	2.075	2.75	1325.3
		0.034			
		0.01			
		1.44			
		0.074			
		0.659			
⭐	SG5	0.0002	2.575	2.94	1141.7
		0.042			
		0.012			
		1.788			

24. Surface wettability characterization
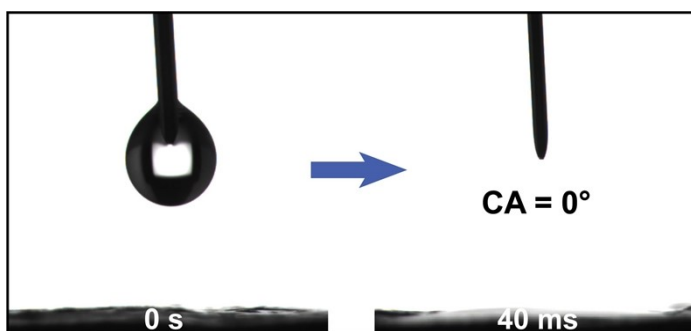
Figure S21. Water contact angle (CA) measurements of CNF-SA-PVA aerogels.

25. Density and porosity characterization
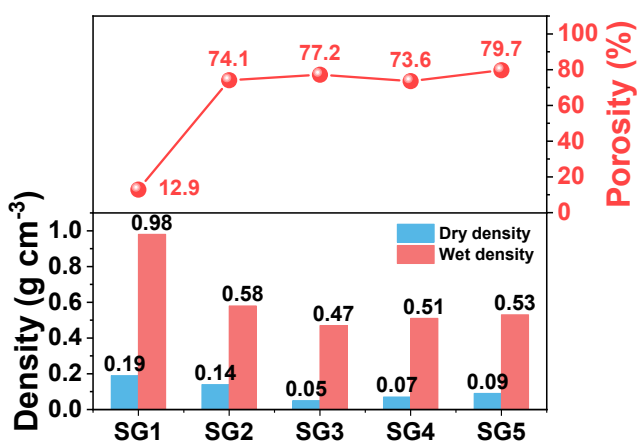
Figure S22. Density and porosity measurements of SG1−SG5.

26. SEM images
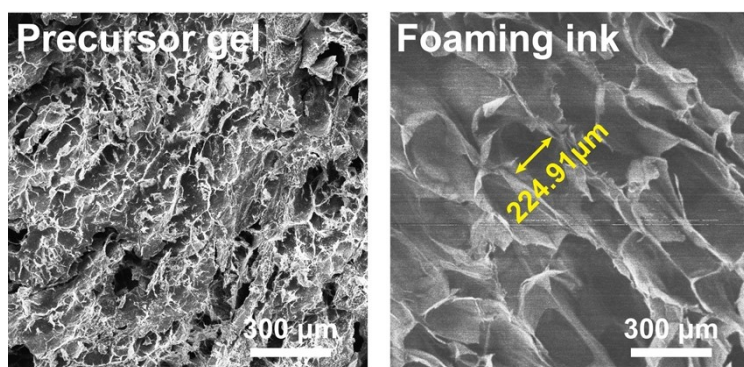
Figure S23. SEM images of aerogels fabricated through the precursor gel and foaming ink.

27. COMSOL simulation
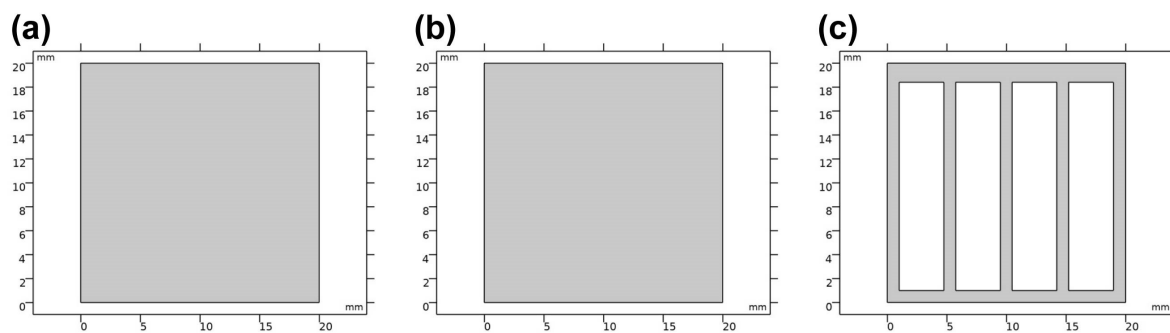
Figure S24. Geometry modeling of (a) SG1, (b) SG2 and (c) SG5.
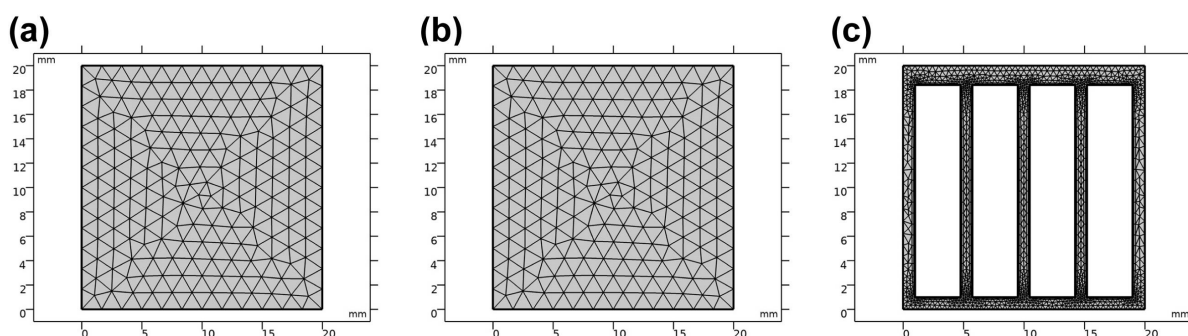
Figure S25. Geometry modeling and meshing of (a) SG1, (b) SG2 and (c) SG5.

28. Energy loss analysis

a) Radiation loss:

The radiation loss was analyzed by Stefan-Boltzmann Equation S2,[53]

$$\Phi = \varepsilon A \sigma \left(T_1^4 - T_2^4 \right) \qquad\qquad (S2)$$

Φ is heat flux (W), ε denotes emissivity (Supposing the evaporator has a maximum emissivity of 1), A is evaporation surface area (4 cm^2), σ represents the Stefan-Boltzmann constant ($\sigma = 5.670373 \times 10^{-8}$ W m^{-2} K^{-4}), T_1 is the average surface temperature of the solar absorber after stable steam generation under one-sun illumination (314.15 K for SG-1, 304.45 K for SG-2, 304.65 K for SG-3, 305.25 K for SG-4, 305.95 K for SG-5). T_2 is the ambient temperature around the evaporator (298.15 K). Therefore, based on Equation S2, we can calculate that the radiation heat loss of SG1 is ~10.4%. The radiation heat loss of SG2 is ~3.9%. The radiation heat loss of SG3 is ~4.0%. The radiation heat loss of SG4 is ~4.4%. The radiation heat loss of SG5 is ~4.9%.

b) Conduction loss:

The heat loss of convection was analyzed according to the following Equation S3,[54]

$$Q = Cm\Delta T \qquad\qquad (S3)$$

Q denotes the heat energy, C is the specific heat capacity of pure water (4.2 kJ °C^{-1} kg^{-1}), m represents the weight of bulk water and ΔT is the increased temperature of the bulk water after stable steam generation. In our experimental, m = 45 g, ΔT =0.6 °C for SG1, ΔT = 0.4 °C for SG2, ΔT = 0.2 °C for SG3, ΔT = 0.3 °C for SG4, ΔT = 0.2 °C for SG5. Therefore, based on Equation S3, we can calculate that the conduction heat loss is ~7.9% for SG1, ~5.3% for SG2, ~2.6% for SG3, ~3.9% for SG4, ~2.6% for SG5.

c) Convection loss:

The convection loss was calculated by Newton's law of cooling S4,[55]

$$Q = hA\Delta T \qquad\qquad \text{(S4)}$$

Q is the heat energy, h denotes the convection heat transfer coefficient ($\sim$5 W m^{-2} K^{-1}). A represents surface area. ΔT is difference between the ambient temperature around the evaporator and the surface temperature of the evaporator. Therefore, based on Equation S4, we can calculate that the convection heat loss of SG1 is $\sim$8.0%. The radiation heat loss of SG2 is $\sim$3.2%. The radiation heat loss of SG3 is $\sim$3.3%. The radiation heat loss of SG4 is $\sim$3.6%. The radiation heat loss of SG5 is $\sim$3.9%.

d) Reflection loss:

The solar absorption of solar absorber is 94.1%; thus, the refection loss is $\sim$5.9%.
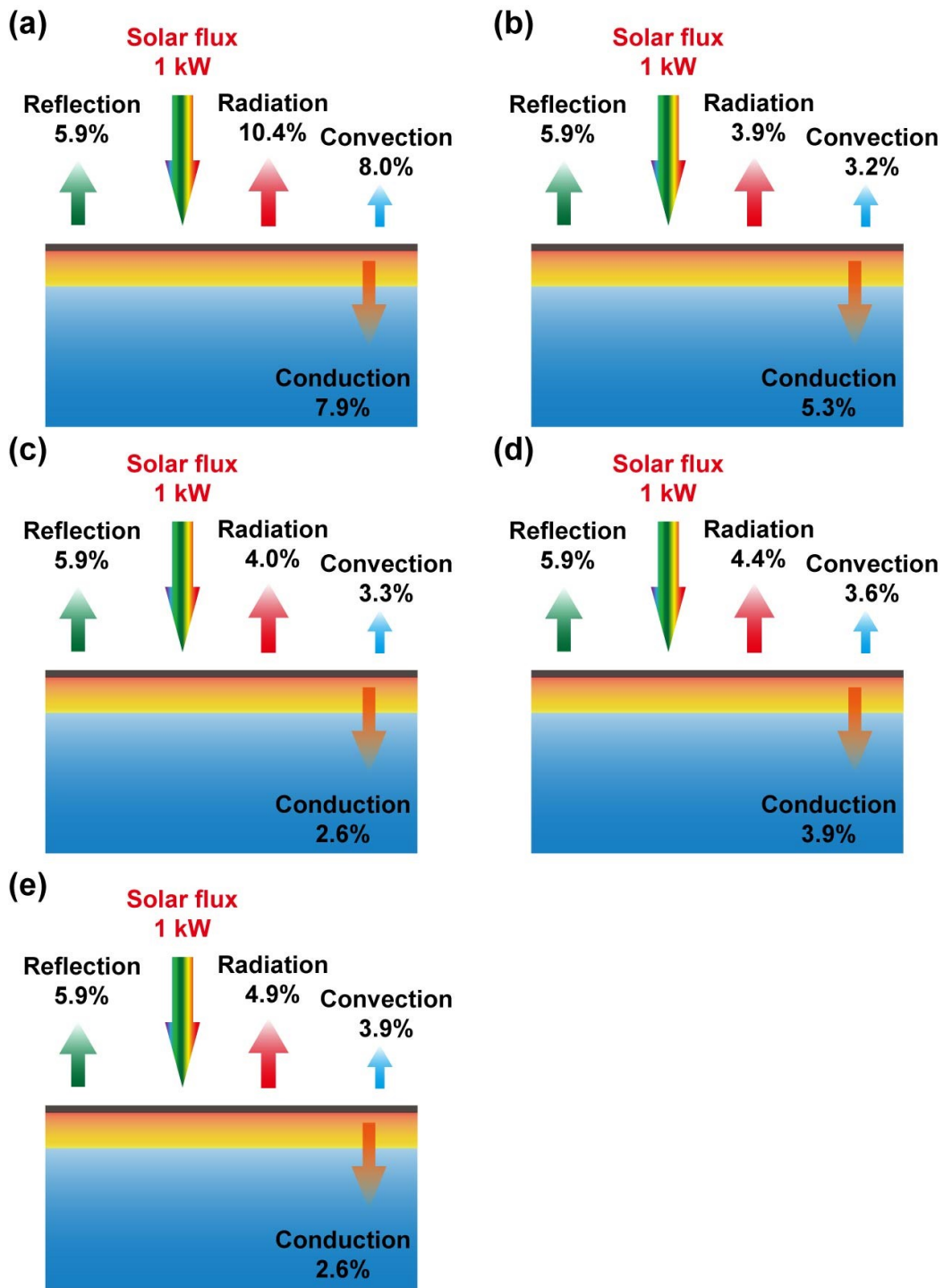
Figure S26. Schematic illustration of solar energy balance and energy transfer pathways of (a) SG1, (b) SG2, (c) SG3, (d) SG4 and (e) SG5.

29. DSC characterization
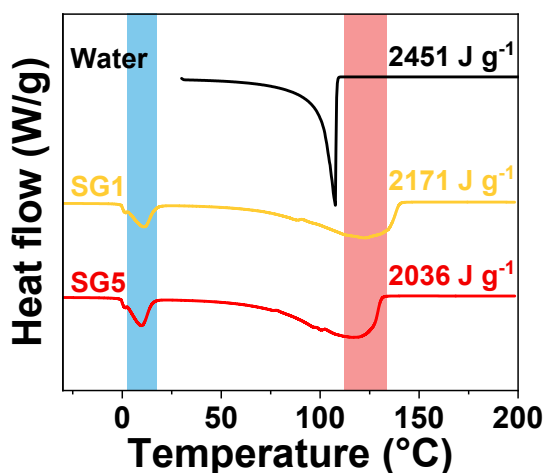
Figure S27. DSC curves of bulk water, and water-saturated SG1 and SG5.

30. Compression testing
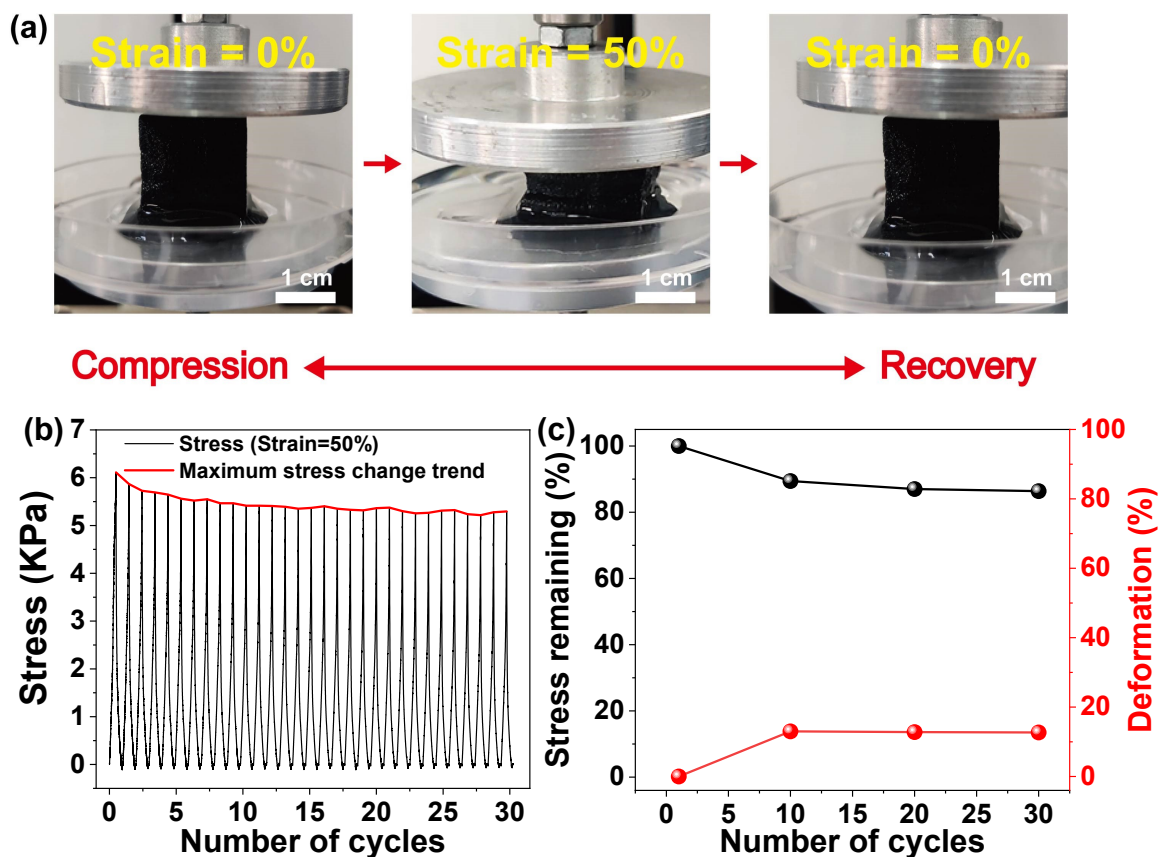
Figure S28. (a) Digital photographs of the SG5 before and after compression. (b) Measured stress of the water-saturated SG5 over loading and releasing cycles at a strain of 50%. (c) Corresponding stress variations and deformation over loading and releasing cycles.

31. Solar desalination characterization
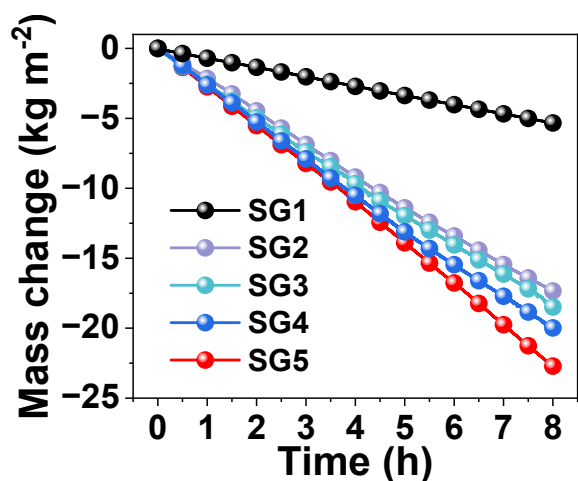
Figure S29. Solar desalination of SG1−SG5 in hypersaline brine with a salinity of 150 g kg^{-1}.

32. Salt exchange characterization
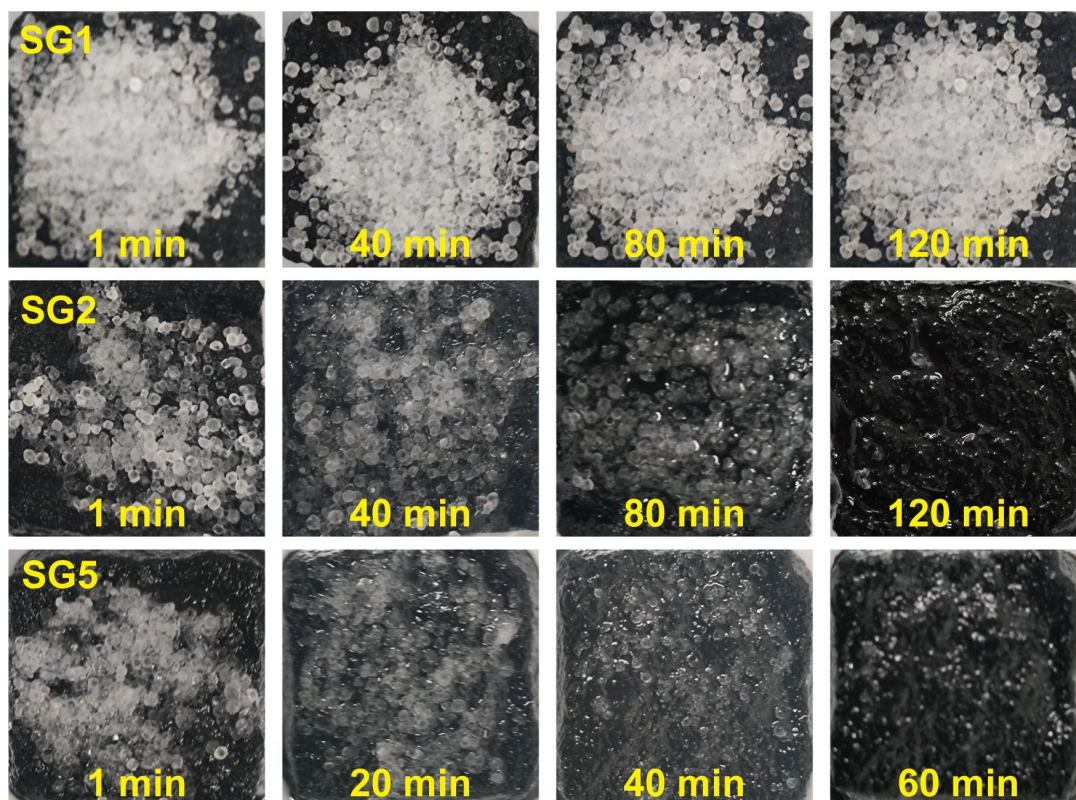
Figure S30. Dissolution of salt crystals on the upper surfaces of SG1, SG2 and SG5.

33. Solar evaporation in outdoor measurements
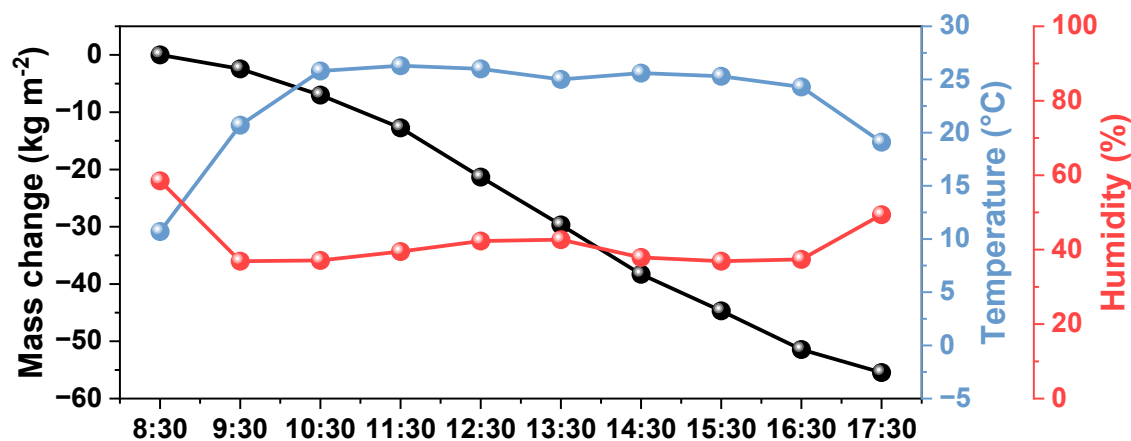
Figure S31. Mass change of SG5, ambient temperature and humidity during outdoor evaporation measurements.
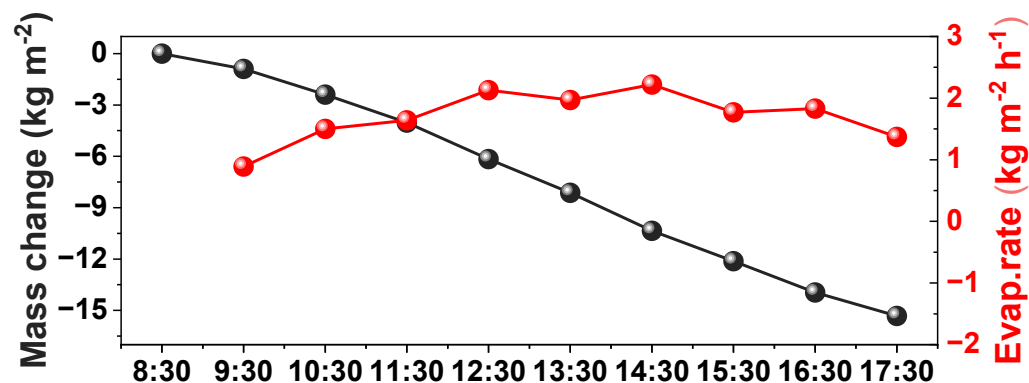
Figure S32. Mass change and evaporation rate of bulk brine during outdoor evaporation measurements.

34. Reference

1. N. Cao, S. Lu, R. Yao, C. Liu, Q. Xiong, W. Qin and X. Wu, *Chem. Eng. J.*, 2020, **397**, 125522.
2. L. Wu, Z. Dong, Z. Cai, T. Ganapathy, N. X. Fang, C. Li, C. Yu, Y. Zhang and Y. Song, *Nat. Commun.*, 2020, **11**, 521.
3. J. Yang, H. Wang, B. Zhou, J. Shen, Z. Zhang and A. Du, *Langmuir*, 2021, **37**, 2129-2139.
4. S. Chaule, J. Hwang, S. J. Ha, J. Kang, J. C. Yoon and J. H. Jang, *Adv. Mater.*, 2021, **33**, 2102649.
5. M. Zou, Y. Zhang, Z. Cai, C. Li, Z. Sun, C. Yu, Z. Dong, L. Wu and Y. Song, *Adv. Mater.*, 2021, **33**, 2102443.
6. W. Jonhson, X. Xu, D. Zhang, W. T. Chua, Y. H. Tan, X. Liu, C. Guan, X. H. Tan, Y. Li, T. S. Herng, J. C. Goh, J. Wang, H. He and J. Ding, *ACS Appl. Mater. Interfaces*, 2021, **13**, 23220-23229.

7. Y. Yang, W. Fan, S. Yuan, J. Tian, G. Chao and T. Liu, *J. Mater. Chem. A*, 2021, **9**, 23968-23976.
8. S. Zhou, S. Huang, Y. Ming, Y. Long, H. Liang, S. Ruan, Y.-J. Zeng and H. Cui, *J. Mater. Chem. A*, 2021, **9**, 9909-9917.
9. J. J. Koh, G. J. H. Lim, S. Chakraborty, Y. Zhang, S. Liu, X. Zhang, S. C. Tan, Z. Lyu, J. Ding and C. He, *Nano Energy*, 2021, **79**, 105436.
10. J. Yuan, X. Lei, C. Yi, H. Jiang, F. Liu and G. J. Cheng, *Chem. Eng. J.*, 2022, **430**, 132765.
11. S. Sun, C. Shi, Y. Kuang, M. Li, S. Li, H. Chan, S. Zhang, G. Chen, A. Nilghaz, R. Cao and J. Tian, *Water Res.*, 2022, **226**, 119279.
12. S. Tang, X. Lu, P. Geng, D. Chen, Y. Shi, J. Su, Y. Zhou, B. Su and S. Wen, *Mater. Adv.*, 2023, **4**, 223-230.
13. L. Chen, S. He, W. Huang, D. Liu, T. Bi, C. Zhang and C. Chen, *Compos. B. Eng.*, 2023, **263**, 110830.
14. P. Zhu, Z. Yu, H. Sun, D. Zheng, Y. Zheng, Y. Qian, Y. Wei, J. Lee, S. Srebnik, W. Chen, G. Chen and F. Jiang, *Adv. Mater.*, 2023, 2306653.
15. C. Shi, X. Zhang, A. Nilghaz, Z. Wu, T. Wang, B. Zhu, G. Tang, B. Su and J. Tian, *Chem. Eng. J.*, 2023, **455**, 140361.
16. R. Fillet, V. Nicolas, A. Celzard and V. Fierro, *Chem. Eng. J.*, 2023, **457**, 141168.
17. X. Zhang, Y. Yan, N. Li, P. Yang, Y. Yang, G. Duan, X. Wang, Y. Xu and Y. Li, *Sci. Bull.*, 2023, **68**, 203-213.
18. Y. Liu, J. Guo, J.-W. Wang, L. Han, L. Zhu and S. Chen, *Chem. Eng. J.*, 2023, **467**, 143389.
19. T. Cui, W. Cai, F. Chu, Z. Li, Y. Zheng, Z. Gui and Y. Hu, *Chem. Eng. J.*, 2023, **451**, 139102.
20. H. Yang, D. Li, X. Zheng, J. Zuo, B. Zhao, D. Li, J. Zhang, Z. Liang, J. Jin, S. Ju, M. Peng, Y. Sun and L. Jiang, *Adv. Mater.*, 2023, **35**, 2304699.
21. L. Zhang, Y. Zhang, M. Zou, C. Yu, C. Li, C. Gao, Z. Dong, L. Wu and Y. Song, *Adv. Funct. Mater.*, 2023, **33**, 2300318.
22. Z. Wu, D. Sun, C. Shi, S. Chen, S. Tang, Y. Li, C. Yan, Y. Shi and B. Su, *Adv. Funct. Mater.*, 2023, **33**, 2304897.
23. Y. Liu, B. Luo, H. Liu, M. He, R. Wang, L. Wang, Z. Quan, J. Yu and X. Qin, *Chem. Eng. J.*, 2023, **452**, 139402.
24. Z. Jin, M. Zhang, H. Mei, H. Liu, L. Pan, Y. Yan, L. Cheng and L. Zhang, *Carbon*, 2023, **202**, 159-168.
25. X. Zheng, Y. Bao, A. Huang, G. Qin and M. He, *Sep. Purif. Technol.*, 2023, **306**, 122741.
26. Z. Zhan, L. Chen, C. Wang, Y. Shuai, H. Duan and Z. Wang, *ACS Appl. Mater. Interfaces*, 2023, **15**, 8181-8189.
27. X. Su, D. Hao, P. Li, M. Yang, X. Guo, X. Ai, T. Zhao and L. Jiang, *J. Mater. Chem. A*, 2023, **11**, 7702-7710.
28. N. Li, K. Shao, J. He, S. Wang, S. Li, X. Wu, J. Li, C. Guo, L. Yu, P. Murto, J. Chen and X. Xu, *Small*, 2023, **19**, 2301474.
29. J. Zhu, J. Liu, J. Liu, S. Guo, S. Lu, Y. Lv and B. Song, *Desalination*, 2023, **548**, 116275.
30. Z. Wu, C. Shi, Y. Li, A. Chen, L. Chen and B. Su, *Chem. Eng. J.*, 2023, **464**, 142778.
31. Y. Fan, W. Bai, P. Mu, Y. Su, Z. Zhu, H. Sun, W. Liang and A. Li, *Sol. Energy Mater Sol. Cells*, 2020, **206**, 110347.
32. C. Liu, C. Cai, F. Ma, X. Zhao and H. Ahmad, *J. Colloid Interface Sci.*, 2020, **560**, 103-110.
33. S. Wang, C. Xiao, S. Lu, H. Lu, Q.-M. Hasi, Y. Zhang, X. Luo and L. Chen, *ACS Sustain. Chem. Eng.*, 2023, **11**, 2586-2598.

34. Y. Guo, X. Zhou, F. Zhao, J. Bae, B. Rosenberger and G. Yu, *ACS Nano*, 2019, **13**, 7913-7919.
35. J. Xiao, Y. Guo, W. Luo, D. Wang, S. Zhong, Y. Yue, C. Han, R. Lv, J. Feng, J. Wang, W. Huang, X. Tian, W. Xiao and Y. Shen, *Nano Energy*, 2021, **87**, 106213.
36. F. Zhao, X. Zhou, Y. Shi, X. Qian, M. Alexander, X. Zhao, S. Mendez, R. Yang, L. Qu and G. Yu, *Nat. Nanotechnol.*, 2018, **13**, 489-495.
37. N. Wei, Z. Li, Q. Li, E. Yang, R. Xu, X. Song, J. Sun, C. Dou, J. Tian and H. Cui, *J. Colloid Interface Sci.*, 2021, **588**, 369-377.
38. Y. Wang, J. Nie, Z. He, Y. Zhi, X. Ma and P. Zhong, *ACS Appl. Mater. Interfaces*, 2022, **14**, 5876-5886.
39. X. Wang, Q. Liu, S. Wu, B. Xu and H. Xu, *Adv. Mater.*, 2019, **31**, 1807716.
40. X. Wang, Z. Li, Y. Wu, H. Guo, X. Zhang, Y. Yang, H. Mu and J. Duan, *ACS Appl. Mater. Interfaces*, 2021, **13**, 10902-10915.
41. H. Zhou, C. Xue, Q. Chang, J. Yang and S. Hu, *Chem. Eng. J.*, 2021, **421**, 129822.
42. Y. Guo, H. Lu, F. Zhao, X. Zhou, W. Shi and G. Yu, *Adv. Mater.*, 2020, **32**, 1907061.
43. B. Luo, J. Wen, H. Wang, S. Zheng, R. Liao, W. Chen, O. Mahian and X. Li, *Energy Environ. Mater.*, 2022, **6**, e12353.
44. Z. Wang, X. Wu, J. Dong, X. Yang, F. He, S. Peng and Y. Li, *Chem. Eng. J.*, 2022, **427**, 130905.
45. Y. Zhang, W. Deng, M. Wu, Z. Liu, G. Yu, Q. Cui, C. Liu, P. Fatehi and B. Li, *ACS Appl. Mater. Interfaces*, 2023, **15**, 7414-7426.
46. D. P. Storer, J. L. Phelps, X. Wu, G. Owens, N. I. Khan and H. Xu, *ACS Appl. Mater. Interfaces*, 2020, **12**, 15279-15287.
47. Y. Xu, X. Xiao, X. Fan, Y. Yang, C. Song, Y. Fan and Y. Liu, *J. Mater. Chem. A*, 2020, **8**, 24108-24116.
48. B. C. pattnayak and S. Mohapatra, *J. Environ. Chem. Eng.*, 2022, **10**, 108616.
49. Q. Zhao, Z. Huang, S. Tian, X. Cui, Y. Wan, X. Li, Y. Xiao, S. Li and C. S. Lee, *Mater. Today Energy*, 2020, **18**, 100498.
50. X. Lu, J. Tang, Z. Song, H. Wang, D. Yu, G. Li, W. Li and W. Liu, *Sol Energy*, 2022, **231**, 828-836.
51. M. Yin, Y. Hsin, X. Guo, R. Zhang, X. Huang and X. Zhang, *Sci. Total Environ.*, 2021, **759**, 143546.
52. N. Li, L. Luo, C. Guo, J. He, S. Wang, L. Yu, M. Wang, P. Murto and X. Xu, *Chem. Eng. J.*, 2022, **431**, 134144.
53. N. Li, L. Qiao, J. He, S. Wang, L. Yu, P. Murto, X. Li and X. Xu, *Adv. Funct. Mater.*, 2020, **31**, 2008681.
54. J. Zhou, Y. Gu, P. Liu, P. Wang, L. Miao, J. Liu, A. Wei, X. Mu, J. Li and J. Zhu, *Adv. Funct. Mater.*, 2019, **29**, 1903255.
55. X. Li, B. Zhu and J. Zhu, *Carbon*, 2019, **146**, 320-328.